Endoplasmic Reticulum Stress Links Obesity, Insulin Action, and Type 2 Diabetes

Umut Özcan,[1]* Qiong Cao,[1]* Erkan Yilmaz,[1] Ann-Hwee Lee,[2] Neal N. Iwakoshi,[2] Esra Özdelen,[1] Gürol Tuncman,[1] Cem Görgün,[1] Laurie H. Glimcher,[2,3] Gökhan S. Hotamisligil[1]†

Obesity contributes to the development of type 2 diabetes, but the underlying mechanisms are poorly understood. Using cell culture and mouse models, we show that obesity causes endoplasmic reticulum (ER) stress. This stress in turn leads to suppression of insulin receptor signaling through hyperactivation of c-Jun N-terminal kinase (JNK) and subsequent serine phosphorylation of insulin receptor substrate–1 (IRS-1). Mice deficient in X-box–binding protein–1 (XBP-1), a transcription factor that modulates the ER stress response, develop insulin resistance. These findings demonstrate that ER stress is a central feature of peripheral insulin resistance and type 2 diabetes at the molecular, cellular, and organismal levels. Pharmacologic manipulation of this pathway may offer novel opportunities for treating these common diseases.

The cluster of pathologies known as metabolic syndrome, including obesity, insulin resistance, type 2 diabetes, and cardiovascular disease, has become one of the most serious threats to human health. The dramatic increase in the incidence of obesity in most parts of the world has contributed to the emergence of this disease cluster, particularly insulin resistance and type 2 diabetes. However, understanding the molecular mechanisms underlying these individual disorders and their links with each other has been challenging.

Over the past decade, it has become clear that obesity is associated with the activation of cellular stress signaling and inflammatory pathways (1–4). However, the origin of this stress is not known. A key player in the cellular stress response is the ER, a membranous network that functions in the synthesis and processing of secretory and membrane proteins. Certain pathological stress conditions disrupt ER homeostasis and lead to accumulation of unfolded or misfolded proteins in the ER lumen (5–7). To cope with this stress, cells activate a signal transduction system linking the ER lumen with the cytoplasm and nucleus, called the unfolded protein response (UPR) (5–7). Among the

conditions that trigger ER stress are glucose or nutrient deprivation, viral infections, lipids, increased synthesis of secretory proteins, and expression of mutant or misfolded proteins (8–10).

Several of these conditions occur in obesity. Specifically, obesity increases the demand on the synthetic machinery of the cells in many secretory organ systems. Obesity is also associated with mechanical stress, excess lipid accumulation, abnormalities in intracellular energy fluxes, and nutrient availability. In light of these observations, we postulated that obesity may be a chronic stimulus for ER stress in peripheral tissues and that perhaps ER stress is a core mechanism involved in triggering insulin resistance and type 2 diabetes.

Induction of ER stress in obesity. To examine whether ER stress is increased in obesity, we investigated the expression patterns of several molecular indicators of ER stress in dietary [high-fat diet (HFD)–induced] and genetic (*ob/ob*) models of murine obesity. The pancreatic ER kinase or PKR-like kinase (PERK) is an ER transmembrane protein kinase that phosphorylates the α subunit of translation initiation factor 2 (eIF2α) in response to ER stress. The phosphorylation status of PERK and eIF2α is therefore a key indicator of the presence of ER stress (11–13). We determined the phosphorylation status of PERK (Thr^{980}) and eIF2α (Ser^{51}) using phospho-specific antibodies. These experiments demonstrated increased PERK and eIF2α phosphorylation in liver extracts of obese

mice compared with lean controls (Fig. 1, A and B). The activity of c-Jun N-terminal kinase (JNK) is also increased by ER stress (14). Consistent with earlier observations (3), total JNK activity, indicated by c-Jun phosphorylation, was also dramatically elevated in the obese mice (Fig. 1, A and B).

The 78-kD glucose-regulated/binding immunoglobulin protein (GRP78) is an ER chaperone whose expression is increased upon ER stress (7). The GRP78 mRNA levels were elevated in the liver tissue of obese mice compared with matched lean controls (Fig. 1, C and D). Because GRP78 expression is responsive to glucose (15), we tested whether this up-regulation might simply be due to increasing glucose levels. Treatment of cultured rat Fao liver cells with high levels of glucose resulted in reduced GRP78 expression (fig. S1A). Similarly, GRP78 levels were not increased in a mouse model of hyperglycemia (fig. S1B), which indicates that regulation in obesity is unlikely to be related to glycemia alone.

We also tested adipose and muscle tissues, important sites for metabolic ho-
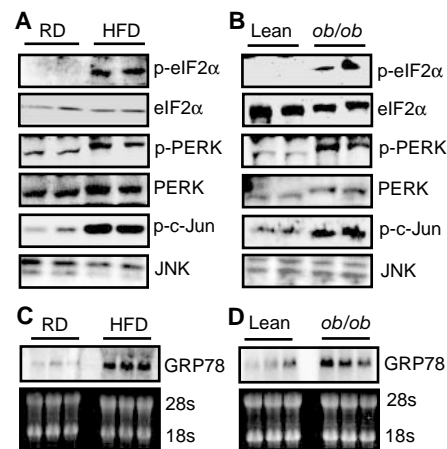
Fig. 1. Increased ER stress in obesity. Dietary (HFD-induced) and genetic (*ob/ob*) models of mouse obesity were used to examine markers of ER stress in liver tissue compared with age- and sex-matched lean controls. (**A**) ER stress markers including eIF2α phosphorylation (p-eIF2α), PERK phosphorylation (p-PERK), and JNK activity (p-c-Jun) were examined in the liver samples of the male mice (C57BL/6) that were kept either on regular diet (RD) or high-fat diet (HFD) for 16 weeks. (**B**) Examination of the same ER stress markers in the livers of male *ob/ob* and wild-type (WT) lean mice at the age of 12 to 14 weeks. (**C**) Northern blot analysis of GRP78 mRNA in the livers of mice with dietary-induced obesity and lean controls. (**D**) Northern blot analysis of GRP78 mRNA in the livers of *ob/ob* and WT lean mice. Ethidium bromide staining is shown as a control for loading and integrity of RNA.

[1]Department of Genetics and Complex Diseases, [2]Department of Immunology and Infectious Diseases, Harvard School of Public Health, [3]Department of Medicine, Harvard Medical School, Boston, MA 02115, USA.

*These authors contributed equally to this work.
†To whom correspondence should be addressed. E-mail: ghotamis@hsph.harvard.edu

meostasis, for indications of ER stress in obesity. As in liver, PERK phosphorylation, JNK activity, and GRP78 expression were all significantly increased in adipose tissue of obese animals compared with lean controls (fig. S2, A to C). However, no indication for ER stress was evident in the muscle tissue of obese animals (16). Taken together, these results indicate that obesity is associated with induction of ER stress predominantly in liver and adipose tissues.

ER stress inhibits insulin action in liver cells. To investigate whether ER stress interferes with insulin action, we pretreated Fao liver cells with tunicamycin or thapsigargin, agents commonly used to induce ER stress. Tunicamycin significantly decreased insulin-stimulated tyrosine phosphorylation

of insulin receptor substrate 1 (IRS-1) (Fig. 2, A and B), and it also produced an increase in the molecular weight of IRS-1 (Fig. 2A). IRS-1 is a substrate for insulin receptor tyrosine kinase, and serine phosphorylation of IRS-1, particularly mediated by JNK, reduces insulin receptor signaling (3). Pretreatment of Fao cells with tunicamycin produced a significant increase in serine phosphorylation of IRS-1 (Fig. 2, A and B). Tunicamycin pretreatment also suppressed insulin-induced Akt phosphorylation, a more distal event in the insulin receptor signaling pathway (Fig. 2, A and B). Similar results were also obtained after treatment with thapsigargin (fig. S3A), which was independent of alterations in cellular calcium levels (fig. S3B). Hence, experimental ER stress inhibits insulin action.

We next examined the role of JNK in ER stress–induced IRS-1 serine phosphorylation and inhibition of insulin-stimulated IRS-1 tyrosine phosphorylation. Inhibition of JNK activity with the synthetic inhibitor, SP600125 (17), reversed the ER stress–induced serine phosphorylation of IRS-1 (Fig. 2, C and D). Pretreatment of Fao cells with a highly specific inhibitory peptide derived from the JNK-binding protein, JIP (18), also completely preserved insulin receptor signaling in cells exposed to tunicamycin (Fig. 2, E and F). Similar results were obtained with the synthetic JNK inhibitor, SP600125 (16). These results indicate that ER stress promotes a JNK-dependent serine phosphorylation of IRS-1, which in turn inhibits insulin receptor signaling.
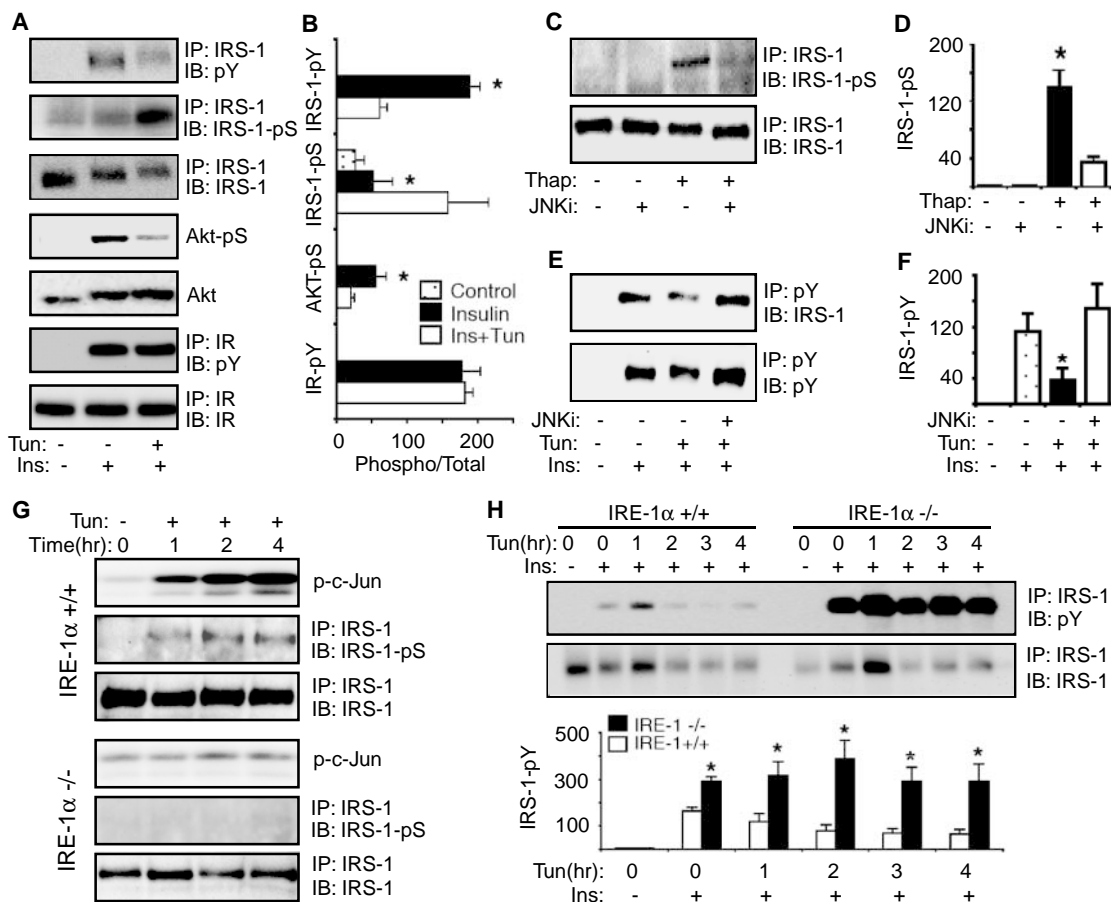
Fig. 2. Induction of ER stress impairs insulin action through JNK-mediated phosphorylation of IRS-1. (**A**) ER stress was induced in Fao liver cells by a 3-hour treatment with 5 μg/ml tunicamycin (Tun). Cells were subsequently stimulated with insulin (Ins). IRS-1 tyrosine (pY) and Ser[307] (pS) phosphorylation, Akt Ser[473] (Akt-pS) phosphorylation, insulin receptor (IR) tyrosine phosphorylation, and their total protein levels were examined either with immunoprecipitation (IP) followed by immunoblotting (IB) or by direct immunoblotting. (**B**) Quantification of IRS-1 (tyrosine and Ser[307]), Akt (Ser[473]), and IR (tyrosine) phosphorylation under the experimental conditions described in (A) with normalization to protein levels for each molecule. (**C**) Inhibition of ER stress–induced (300 nM thapsigargin for 4 hours) Ser[307] phosphorylation of IRS-1 by JNK-1 inhibitor, SP600125 (JNKi, 25 μM). (**D**) Quantification of IRS-1 Ser[307] phosphorylation under the conditions

described in (C). (**E**) Reversal of ER stress–induced inhibition of insulin-stimulated tyrosine phosphorylation (pY) of IRS-1 by a peptide JNK inhibitor. (**F**) Quantification of insulin-induced IRS-1 tyrosine phosphorylation levels described in (E). (**G**) JNK activity (p-c-Jun), Ser[307] phosphorylation of IRS-1, and total IRS-1 levels at indicated times after tunicamycin treatment (Tun, 10 μg/ml) in IRE-1α^{+/+} and IRE-1α^{−/−} fibroblasts. (**H**) Insulin-stimulated IRS-1 tyrosine phosphorylation and total IRS-1 levels after tunicamycin treatment (Tun, 10 μg/ml) in IRE-1α^{+/+} and IRE-1α^{−/−} fibroblasts. Quantification of insulin-induced IRS-1 tyrosine phosphorylation levels in IRE-1α^{+/+} and IRE-1α^{−/−} cells is displayed in the bottom of the panel. All graphs show means ± SEM from at least two independent experiments, and statistical significance (P < 0.005) from the controls is indicated by an asterisk (*).

Inositol-requiring kinase–1α (IRE-1α) plays a crucial role in insulin receptor signaling. In the presence of ER stress, increased phosphorylation of IRE-1α leads to recruitment of tumor necrosis factor receptor–associated factor 2 (TRAF2) protein and activation of JNK (14). To address whether ER stress–induced insulin resistance is dependent on intact IRE-1α, we measured JNK activation, IRS-1 serine phosphorylation, and insulin receptor signaling after exposure of IRE-1α^{−/−} and wild-type fibroblasts to tunicamycin. In the wild-type, but

not IRE-1α^{−/−} cells, induction of ER stress by tunicamycin resulted in strong activation of JNK (Fig. 2G). Tunicamycin also stimulated phosphorylation of IRS-1 at the Ser[307] residue in wild-type, but not IRE-1α^{−/−}, fibroblasts (Fig. 2G). It is noteworthy that tunicamycin inhibited insulin-stimulated tyrosine phosphorylation of IRS-1 in the wild-type cells, whereas no such effect was detected in the IRE-1α^{−/−} cells (Fig. 2H). The level of insulin-induced tyrosine phosphorylation of IRS-1 was dramatically higher in IRE-1α^{−/−} cells, despite lower

total IRS-1 protein levels (Fig. 2H). These results demonstrate that ER stress–induced inhibition of insulin action is mediated by an IRE-1α– and JNK–dependent protein kinase cascade.

**Manipulation of X-box–binding protein–1 (XBP-1) levels alters insulin receptor signaling.** The transcription factor XBP-1 is a bZIP protein. The spliced or processed form of XBP-1 (XBP-1s) is a key factor in ER stress through transcriptional regulation of an array of genes, including molecular chaperones (19–22). We therefore reasoned that modulation of XBP-1s levels in cells should alter insulin action via its potential impact on the magnitude of the ER stress responses. To test this possibility, we established XBP-1 gain- and loss-of-function cellular models. First, we established an inducible gene expression system where exogenous XBP-1s is expressed only in the absence of tetracycline/doxycycline (Fig. 3A). In parallel, we also studied mouse embryo fibroblasts (MEFs) derived from XBP-1^{−/−} mice (Fig. 3B). In fibroblasts without exogenous XBP-1s expression, tunicamycin treatment (2 μg/ml) resulted in PERK phosphorylation starting at 30 min and peaking at 3 to 4 hours, associated with a mobility shift characteristic of PERK phosphorylation (Fig. 3C). In these cells, there was also a rapid and robust activation of JNK in response to ER stress (Fig. 3C). When XBP-1s expression was induced, there was a dramatic reduction in both PERK phosphorylation and JNK activation after tunicamycin treatment (Fig. 3C). Hence, overexpression of XBP-1s rendered wild-type cells refractory to ER stress. Similar experiments performed in XBP-1^{−/−} MEFs revealed an opposite pattern (Fig. 3D). XBP-1^{−/−} MEFs mounted strong ER stress responses even when treated with a low dose of tunicamycin (0.5 μg/ml), which failed to stimulate significant ER stress in wild-type cells (Fig. 3D). Under these conditions, PERK phosphorylation and JNK activation levels in XBP-1^{−/−} MEFs were significantly higher than those seen in wild-type controls (Fig. 3D), which indicates that XBP-1^{−/−} cells are prone to ER stress. Thus, alterations in the levels of cellular XBP-1s protein result in alterations in the ER stress responses.

Next, we examined whether these differences in the ER stress responses produced alterations in insulin action as assessed by IRS-1 serine phosphorylation and insulin-stimulated IRS-1 tyrosine phosphorylation. Tunicamycin-induced IRS-1 serine phosphorylation was significantly reduced in fibroblasts exogenously expressing XBP-1s, compared with that of control cells (Fig. 3E). On insulin stimulation, the extent of IRS-1 tyrosine phosphorylation was significantly
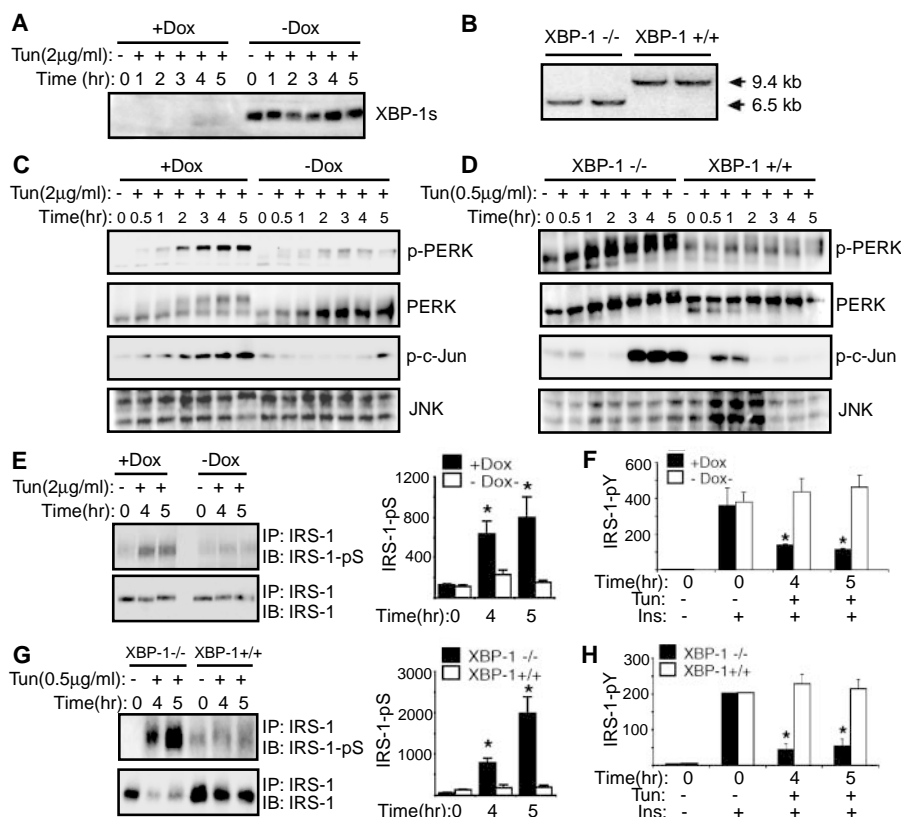
Fig. 3. Alteration of the ER stress response by manipulation of XBP-1 levels modulates insulin receptor signaling. ER stress responses in cells overexpressing XBP-1s, XBP-1^{−/−} cells, and their controls. (**A**) Induction of exogenous XBP-1s expression on removal of doxycycline in MEFs. (**B**) Southern blot analysis of XBP-1^{−/−} MEFs and their WT controls (9.4 kb) and targeted (6.5 kb) alleles. (**C**) PERK phosphorylation (p-PERK) and JNK activity (p-c-Jun) in cells overexpressing XBP-1s and control cells (−Dox and +Dox, respectively) after tunicamycin treatment (Tun, 2 μg/ml). (**D**) PERK phosphorylation and JNK activity after low-dose tunicamycin treatment (Tun, 0.5 μg/ml) in XBP-1^{−/−} MEFs and their WT controls. (**E**) IRS-1 Ser[307] phosphorylation (pS) after tunicamycin treatment (Tun, 2 μg/ml) in cells overexpressing XBP-1s and control cells (−Dox and +Dox, respectively), detected by using immunoprecipitation (IP) of IRS-1 followed by immunoblotting (IB) with an IRS-1 phosphoserine 307–specific antibody. The graph next to the blots shows the quantification of IRS-1 Ser[307] phosphorylation under the conditions described in (E). (**F**) Insulin-stimulated tyrosine phosphorylation of IRS-1 in cells overexpressing XBP-1s and control cells, with or without tunicamycin treatment (Tun, 2 μg/ml). The ratio of IRS-1 tyrosine phosphorylation to total IRS-1 level was summarized from independent experiments and presented in the graph. (**G**) IRS-1 Ser[307] phosphorylation after tunicamycin treatment (Tun, 0.5 μg/ml) in XBP-1^{−/−} cells and WT controls was detected as described in (C). The graph next to the blots shows the quantification of IRS-1 Ser[307] phosphorylation under conditions described in (G). (**H**) Insulin-stimulated tyrosine phosphorylation of IRS-1 in XBP-1^{−/−} and WT control cells with or without tunicamycin treatment (Tun, 0.5 μg/ml). The ratio of IRS-1 tyrosine phosphorylation to total IRS-1 level was summarized from independent experiments and presented in the graph. All graphs show means ± SEM from at least two independent experiments, and statistical significance from the controls is indicated by * with $P < 0.005$.

Fig. 4. Glucose homeostasis in XBP-1$^{+/-}$ mice fed HFD. The XBP-1$^{+/-}$ ($\Diamond$) and XBP-1$^{+/+}$ ($\blacksquare$) mice were fed HFD immediately after weaning at 3 weeks of age. Total body weight (**A**), fasting blood insulin (**B**), C-peptide (**C**), and glucose (**D**) levels were measured in the XBP-1$^{+/-}$ and XBP-1$^{+/+}$ mice during the course of HFD. GTT were performed after 7 (**E**) and 16 (**F**) weeks of HFD in XBP-1$^{+/-}$ and XBP-1$^{+/+}$ mice. ITT were performed after 8 (**G**) and 17 (**H**) weeks of HFD in XBP-1$^{+/-}$ ($n = 11$) and XBP-1$^{+/+}$ ($n = 8$) mice. Data are shown as means ± SEM. Statistical significance in two-tailed Student's t test is indicated by *$P \le 0.05$, **$P \le 0.005$, and ***$P \le 0.0005$. XBP-1$^{+/-}$ and XBP-1$^{+/+}$ groups are also compared by ANOVA (A to H).
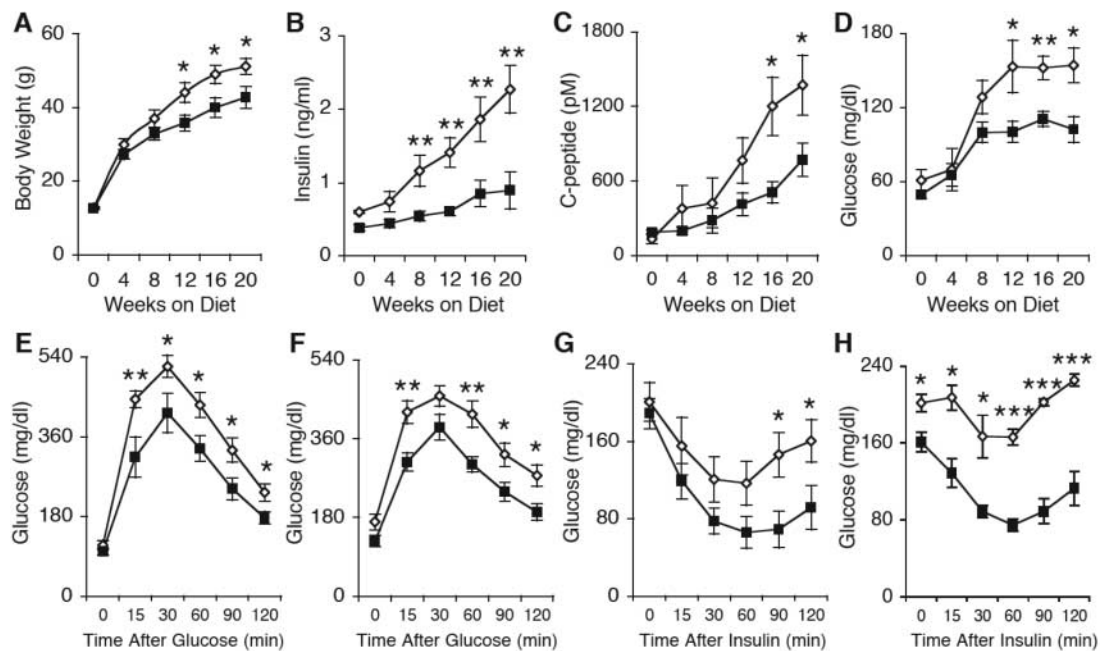
higher in cells overexpressing XBP-1s, compared with controls (Fig. 3F). In contrast, IRS-1 serine phosphorylation was strongly induced in XBP-1$^{-/-}$ MEFs compared with XBP-1$^{+/+}$ controls even at low doses of tunicamycin treatment (0.5 μg/ml) (Fig. 3G). After insulin stimulation, the amount of IRS-1 tyrosine phosphorylation was significantly decreased in tunicamycin-treated XBP-1$^{-/-}$ cells compared with tunicamycin-treated wild-type controls (Fig. 3H). Insulin-stimulated tyrosine phosphorylation of the insulin receptor was normal in these cells (fig. S4).

XBP-1$^{+/-}$ mice show impaired glucose homeostasis. Complete XBP-1 deficiency results in embryonic lethality (23). To investigate the role of XBP-1 in ER stress, insulin sensitivity, and systemic glucose metabolism in vivo, we studied BALB/c-XBP-1$^{+/-}$ mice with a null mutation in one XBP-1 allele. We chose mice on the BALB/c genetic background, because this strain exhibits strong resistance to obesity-induced alterations in systemic glucose metabolism. Based on our results with cellular systems, we hypothesized that XBP-1 deficiency would predispose mice to the development of insulin resistance and type 2 diabetes.

We fed XBP-1$^{+/-}$ mice and their wild-type littermates a HFD at 3 weeks of age. In parallel, control mice of both genotypes were placed on laboratory feed, a regular diet. The total body weights of both genotypes were similar with regular diet and until 12 weeks of age when fed HFD. After this period, the XBP-1$^{+/-}$ animals fed HFD exhibited a small, but significant, increase in body weight (Fig. 4A). Serum levels of leptin, adiponectin, and triglycerides did not exhibit any statistically significant differences between the genotypes measured after 16 weeks of HFD (fig. S5).

Fed HFD, XBP-1$^{+/-}$ mice developed continuous and progressive hyperinsulinemia evident as early as 4 weeks (Fig. 4B). Insulin levels continued to increase in XBP-1$^{+/-}$ mice for the duration of the experiment. Blood insulin levels in XBP-1$^{+/+}$ mice were significantly lower than those in XBP-1$^{+/-}$ littermates (Fig. 4B). C-peptide levels were also significantly higher in XBP-1$^{+/-}$ animals than in wild-type controls (Fig. 4C). Blood glucose levels also began to rise in the XBP-1$^{+/-}$ mice fed HFD starting at 8 weeks and remained high until the conclusion of the experiment at 20 weeks (Fig. 4D). This pattern was the same in both fasted (Fig. 4D) and fed (16) states. The rise in blood glucose in the face of hyperinsulinemia in the mice fed HFD is a strong indicator of the development of peripheral insulin resistance.

To investigate systemic insulin sensitivity, we performed glucose tolerance tests (GTT) and insulin tolerance tests (ITT) in XBP-1$^{+/-}$ mice and XBP-1$^{+/+}$ controls. Exposure to HFD resulted in significant glucose intolerance in XBP-1$^{+/-}$ mice. After 7 weeks of HFD, XBP-1$^{+/-}$ mice showed significantly higher glucose levels on glucose challenge than XBP-1$^{+/+}$ mice (Fig. 4E). This glucose intolerance continued to be evident in XBP-1$^{+/-}$ mice compared with wild-type mice after 16 weeks of HFD (Fig. 4F). During ITT, the hypoglycemic response to insulin was also significantly lower in XBP-1$^{+/-}$ mice compared with XBP-1$^{+/+}$ littermates at 8 weeks of HFD (Fig. 4G), and this reduced responsiveness continued to be evident after 17 weeks of HFD (Fig. 4H). Examination of islets morphology and function did not reveal significant differences between genotypes (fig. S6). Hence, loss of an XBP-1 allele predisposes mice to diet-induced peripheral insulin resistance and type 2 diabetes.

Increased ER stress and impaired insulin signaling in XBP-1$^{+/-}$ mice. Our experiments with cultured cells demonstrated an increase in ER stress and a decrease in insulin signaling capacity in XBP-1–deficient cells, as well as reversal of these phenotypes on expression of high levels of XBP-1s. If this mechanism is the basis of the insulin resistance seen in XBP-1$^{+/-}$ mice, these animals should exhibit high levels of ER stress coupled with impaired insulin receptor signaling. To test this, we first examined PERK phosphorylation and JNK activity in the livers of obese XBP-1$^{+/-}$ and wild-type mice. These experiments revealed an increase in PERK levels and seemingly an increase in liver PERK phosphorylation in obese XBP-1$^{+/-}$ mice compared with wild-type controls fed HFD (Fig. 5A). There was a significant increase in JNK activity in XBP-1$^{+/-}$ mice compared with wild-type controls (Fig. 5B). Consistent with these results, Ser^{307} phosphorylation of IRS-1 was also increased in XBP-1$^{+/-}$ mice compared with wild-type controls fed HFD (Fig. 5C). Finally, we studied in vivo insulin-stimulated, insulin receptor–signaling capacity in these mice.

Fig. 5. ER stress and insulin receptor signaling in XBP-1$^{+/-}$ mice. PERK phosphorylation (p-PERK) (**A**), JNK activity (p-c-Jun) (**B**), and Ser^{307} phosphorylation (pS) of IRS-1 (**C**) were examined in the livers of XBP-1$^{+/-}$ and XBP-1$^{+/+}$ mice after 16 weeks of HFD. After infusion of insulin (1 U/kg) through the portal vein, insulin receptor (IR) tyrosine phosphorylation (pY) (**D**), IRS-1 tyrosine phosphorylation (**E**), IRS-2 tyrosine phosphorylation (**F**), and Akt Ser^{473} phosphorylation (pS) (**G**) were examined in livers of XBP-1$^{+/-}$ and XBP-1$^{+/+}$ mice after 16 weeks of HFD. Total protein levels are shown in the lower point of each panel.
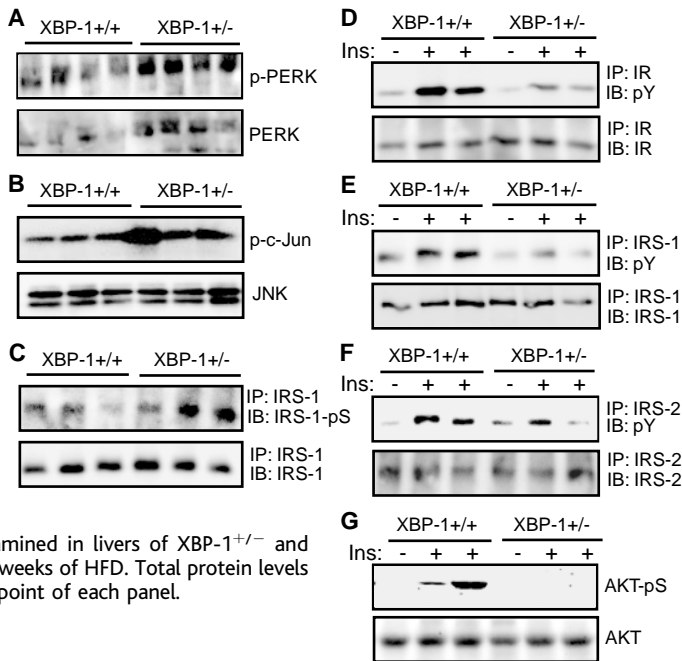
There was no detectable difference in any of the insulin receptor–signaling components in liver and adipose tissues between genotypes taking regular diet (fig. S7). However, after exposure to HFD, major components of insulin receptor signaling in the liver, including insulin-stimulated insulin receptor, IRS-1, and IRS-2 tyrosine- and Akt serine-phosphorylation, were all decreased in XBP-1$^{+/-}$ mice compared with wild-type controls (Fig. 5, D to G). A similar suppression of insulin receptor signaling was also evident in the adipose tissues of XBP-1$^{+/-}$ mice compared with XBP-1$^{+/+}$ mice fed HFD (fig. S8). The suppression of IR tyrosine phosphorylation in XBP-1$^{+/-}$ mice differs from the observations made in XBP-1$^{-/-}$ cells, where ER stress inhibited insulin action after the receptor signal in the pathway. It is likely that this difference reflects the effects of chronic hyperinsulinemia in vivo on insulin receptors. Hence, our data demonstrate the link between ER stress and insulin action in vivo but are not conclusive in determining the exact locus in insulin receptor signaling pathway that is targeted through this mechanism.

Discussion. In this study, we identify ER stress as a molecular link between obesity, the deterioration of insulin action, and the development of type 2 diabetes. Induction of ER stress or reduction in the compensatory capacity through down-regulation of XBP-1 leads to suppression of insulin receptor signaling in intact cells via IRE-1α–dependent activation of JNK. Experiments with mouse models also yielded data consistent with the link between ER stress and systemic insulin action. Deletion of an XBP-1 allele in mice leads to enhanced ER stress, hyperactivation of JNK, reduced insulin receptor signaling, systemic insulin resistance, and type 2 diabetes.

Our findings point to a fundamental mechanism underlying the molecular sensing of obesity-induced metabolic stress by the ER and inhibition of insulin action that ultimately leads to insulin resistance and type 2 diabetes. We therefore postulate that ER stress underlies the emergence of the stress and inflammatory responses in obesity and the integrated deterioration of systemic glucose homeostasis.

Although our results in this study predominantly point to a role for ER stress in peripheral insulin resistance, earlier studies have linked ER stress with islet function and survival. For example, PERK$^{-/-}$ mice exhibit a phenotype resembling type 1 diabetes resulting from pancreatic islet destruction soon after birth (*24*). PERK mutations also cause a rare inherited form of type 1 diabetes in humans (*25*). Loss of eIF2α phosphorylation by targeted mutation of serine 51 residue of eIF2α to alanine also leads to alterations in pancreatic beta cell function, in addition to its impact on liver gluconeogenesis (*11*, *26*). Therefore, we propose that the effect of chronic ER stress on glucose homeostasis in obesity could represent a central and integrating mechanism underlying both peripheral insulin resistance and impaired insulin secretion.

The critical role of ER stress responses in insulin action may represent a mechanism conserved by evolution, whereby stress signals are integrated with metabolic regulatory pathways through the ER. This integration could have been advantageous, because proper regulation of energy fluxes and the suppression of major anabolic pathways might have been favorable during acute stress, pathogen invasion, and immune responses. Hence, the trait would propagate through natural selection. However, in the presence of chronic ER stress, such as we see in obesity, the effect of ER stress on metabolic regulation would lead to the development of insulin resistance and, eventually, type 2 diabetes. In terms of therapeutics, our findings suggest that interventions that regulate the ER stress response offer new opportunities for preventing and treating type 2 diabetes.

References and Notes

1. G. S. Hotamisligil, in *Diabetes Mellitus*, D. LeRoith, S. I. Taylor, J. M. Olefsky, Eds. (Lippincott Williams & Wilkins, Philadelphia, 2003), pp. 953–962.
2. K. T. Uysal, S. M. Wiesbrock, M. W. Marino, G. S. Hotamisligil, *Nature* **389**, 610 (1997).
3. J. Hirosumi *et al.*, *Nature* **420**, 333 (2002).
4. M. Yuan *et al.*, *Science* **293**, 1673 (2001).
5. R. Y. Hampton, *Curr. Biol.* **10**, R518 (2000).
6. K. Mori, *Cell* **101**, 451 (2000).
7. H. P. Harding, M. Calfon, F. Urano, I. Novoa, D. Ron, *Annu. Rev. Cell Dev. Biol.* **18**, 575 (2002).
8. Y. Ma, L. M. Hendershot, *Cell* **107**, 827 (2001).
9. R. J. Kaufman *et al.*, *Nature Rev. Mol. Cell Biol.* **3**, 411 (2002).
10. I. Kharroubi *et al.*, *Endocrinology* (2004); published online 5 August 2004 (10.1210/en.2004-0478).
11. Y. Shi, S. I. Taylor, S. L. Tan, N. Sonenberg, *Endocr. Rev.* **24**, 91 (2003).
12. Y. Shi *et al.*, *Mol. Cell. Biol.* **18**, 7499 (1998).
13. H. P. Harding, Y. Zhang, D. Ron, *Nature* **397**, 271 (1999).
14. F. Urano *et al.*, *Science* **287**, 664 (2000).
15. R. P. Shiu, J. Pouyssegur, I. Pastan, *Proc. Natl. Acad. Sci. U.S.A.* **74**, 3840 (1977).
16. U. Özcan, G. S. Hotamisligil, unpublished observations.
17. B. L. Bennett *et al.*, *Proc. Natl. Acad. Sci. U.S.A.* **98**, 13681 (2001).
18. R. K. Barr, T. S. Kendrick, M. A. Bogoyevitch, *J. Biol. Chem.* **277**, 10987 (2002).
19. M. Calfon *et al.*, *Nature* **415**, 92 (2002).
20. X. Shen *et al.*, *Cell* **107**, 893 (2001).
21. H. Yoshida, T. Matsui, A. Yamamoto, T. Okada, K. Mori, *Cell* **107**, 881 (2001).
22. A. H. Lee, N. N. Iwakoshi, L. H. Glimcher, *Mol. Cell. Biol.* **23**, 7448 (2003).
23. A. M. Reimold *et al.*, *Genes Dev.* **14**, 152 (2000).
24. H. P. Harding *et al.*, *Mol. Cell* **7**, 1153 (2001).
25. M. Delepine *et al.*, *Nature Genet.* **25**, 406 (2000).
26. D. Scheuner *et al.*, *Mol. Cell* **7**, 1165 (2001).
27. We thank the Hotamisligil laboratory for their contributions and J. Gound and L. Beppu for technical assistance. Supported in part by NIH grants AI32412 (L.H.G.), DK52539 (G.S.H.), American Diabetes Association (G.S.H.), PO5-CA100707 (L.H.G., A.H.L.), an Irvington Institute Postdoctoral Fellowship Award (N.I.), an NIH training grant T32-DK07703 (Q.C.), and a postdoctoral fellowship from the Iaccoca Foundation (G.T.). L.H.G. holds equity in MannKind Corporation, which has licensed the XBP-1 technology.